Letter

Temperature-pressure phase diagram of the intrinsically insulating topological antiferromagnet $EuCd_2As_2$

Xuliang Chen (陈绪亮),[1] Shuyang Wang,[1] Jing Wang,[1] Chao An,[2] Ying Zhou,[2] Zheng Chen,[1] Xiangde Zhu,[1] Yonghui Zhou,[1] Zhaorong Yang,[1,2,3,*] and Mingliang Tian[1,2,3,4,†]

[1]*Anhui Province Key Laboratory of Condensed Matter Physics at Extreme Conditions, High Magnetic Field Laboratory, HFIPS, Chinese Academy of Sciences, Hefei 230031, China*

[2]*Institutes of Physical Science and Information Technology, Anhui University, Hefei 230601, China*

[3]*Collaborative Innovation Center of Advanced Microstructures, Nanjing 210093, China*

[4]*School of Physics and Materials Science, Anhui University, Hefei 230601, China*

(Received 15 April 2023; revised 13 June 2023; accepted 14 June 2023; published 26 June 2023)

Zintl-phase $EuCd_2As_2$ attracts much research interest because it has a potential of manifesting various ideal topological states under external parameters. Here, measurements of resistance, magnetization, Hall, and synchrotron x-ray diffraction at high pressures up to 50.8 GPa in diamond anvil cells are performed on high-quality $EuCd_2As_2$ single crystals that display a long-sought intrinsically insulating antiferromagnetic (AFM) ground state. From ambient pressure to 21.0 GPa, the AFM state of $EuCd_2As_2$ is stable and the AFM transition temperature of ∼9.5 K is raised linearly at a rate of ∼1.90 K/GPa. Meanwhile, the insulating conduction behavior is maintained despite that the whole resistance decreases remarkably. Beyond ∼24.0 GPa, a ferromagnetic-like metallic state shows up, due to a trigonal $P\bar{3}m1$ to monoclinic $C2/m$ structural transition, and its transition temperature of ∼150 K increases linearly at a rate of ∼0.69 K/GPa. This high-pressure magnetic metallic state dominates over the pristine AFM insulating one upon completion of the structural transition around 40 GPa. Based on the present data, we construct a temperature-pressure phase diagram for the intrinsically insulating antiferromagnet $EuCd_2As_2$, which offers essential insights into the pressure-dependent evolutions of magnetic and transport properties and will stimulate further exploration of the interplay among magnetism and transport, as well as nontrivial topology rooted in their interactions.

DOI: 10.1103/PhysRevB.107.L241106

Magnetic topological materials attract wide and continuous attention since the interplay of magnetism and nontrivial band topology can generate exotic topological quantum states, including the quantum anomalous Hall effect [1], axion insulator states [2–4], as well as magnetic Weyl semimetals [5,6]. For magnetic topological materials, a variety of nontrivial band topologies depend on different magnetic configurations and thus enables their tunability by controlling their spin texture, which is not only of significant interests in exploring rich and unusual quantum phenomena but also promises great application potentials in spintronic devices [7,8].

Recently, considerable attention was paid to a Zintl-phase antiferromagnetic (AFM) $EuCd_2As_2$ since this material has the potential of manifesting various ideal nontrivial topological states depending on its different magnetic structures [9–16], thus allowing for the use of magnetism to tune the topological properties just within the same host. $EuCd_2As_2$ belongs to a layered trigonal structure (space group $P\bar{3}m1$, No. 164) with Cd_2As_2 bilayers separated by triangle Eu-atom layers. The magnetism of $EuCd_2As_2$ originates from the Eu^{2+} ions. An A-type AFM order below $T_N \sim 9.5$ K was identified [15–17], with an intraplane ferromagnetic (FM) alignment of the Eu^{2+} moments and an interplane AFM superexchange interaction. From the band-topology perspective, $EuCd_2As_2$ was proposed as an AFM topological semimetal with the simplest double-cone structure near the Fermi level [14] and an ideal FM Weyl semimetal featuring a single pair of Weyl points [11,12,15] when the Eu^{2+} moments are forced to align out of plane (parallel to the c axis) under modest applied c-axis magnetic fields. In addition, alloying with Ba at the Eu site [18,19] can generate an FM state in $EuCd_2As_2$, which may make the ideal Weyl physics accessible even without external magnetic fields. Overall, these results point to the close proximity in energy between the readily transformable AFM and FM states and magnetic exchange-induced ideal topological states in $EuCd_2As_2$.

Considering that the strength of magnetic exchange coupling in $EuCd_2As_2$ depends on the separation of the Eu^{2+} ions, thus it would be of interest to manipulate its magnetism and thereby band topology by using external pressure as the tuning knob. Indeed, there have been several reports on pressure tuning of magnetic and transport properties of $EuCd_2As_2$ [20–22]. Nevertheless, clear discrepancies especially in transport measurements under pressure were observed. This may be related to quality of the starting samples used because the intrinsic transport behavior of topological insulators is highly susceptible to the chemical potential or band filling, an issue that is commonly encountered in topological insulators like $Bi_2Se(Te)_3$ [23]. As a well-known Zintl-phase material that will be valence precise if charges transfer completely

*Corresponding author: zryang@issp.ac.cn
†Corresponding author: tianml@hmfl.ac.cn

 ©2023 American Physical Society

from cations to anionic slabs, $EuCd_2As_2$ is expected to be a insulator/semiconductor or an AFM topological insulator (axion insulator) by taking magnetism into account [11,14]. However, almost all previously reported transport experiments found that at ambient pressure $EuCd_2As_2$ manifests a metallic conduction behavior at high temperature, followed by a sharp peak feature centered at the AFM transition temperature T_N [12,18,24]. Namely, $EuCd_2As_2$ was widely viewed as an AFM topological semimetal. Very recently, $EuCd_2As_2$ was confirmed as a magnetic semiconductor at ambient pressure [25]. Under such circumstance, it is highly desirable to first obtain intrinsically insulating AFM $EuCd_2As_2$ single crystals and then systematically investigate their high-pressure properties.

In this Letter, we present a systematic high-pressure study of intrinsically insulating antiferromagnet $EuCd_2As_2$ by a combination of electrical resistance, Hall effect, and synchrotron x-ray diffraction (XRD) measurements in diamond anvil cells (DACs) with pressures up to 49.5 GPa. We found that the AFM state and the insulating conduction are stable against pressure to around 21.0 GPa, above which a FM-like metallic state shows up as signified by the occurrence of anomalous Hall effect. Both the AFM- and FM-like-transition temperatures T_N and T_C increases linearly with pressure. The transition from the AFM insulating state to FM-like metallic state is due to a trigonal $P\bar{3}m1$ to monoclinic $C2/m$ structural transition. As such, an intrinsic temperature-pressure phase diagram for this material is constructed.

High-quality single crystals of $EuCd_2As_2$ with an insulating AFM ground state were grown by melting method using Bi as the flux. High-pressure resistance and Hall effect measurements were performed in a Be-Cu alloy DAC by using an in-house multifunctional physical properties measurement system. The details of sample loading in DAC and data processing procedures for transport experiments are similar to those reported previously [26]. The DC magnetization (M) measurement at high pressures was performed on the SQUID-VSM-7T (Quantum Design, MPMS3) equipped with Be-Cu alloy DAC (the culet size is 500 μm). The room-temperature angle-dispersive synchrotron XRD experiments were carried out on fine powders of well-ground $EuCd_2As_2$ single crystals by using a Mao-type DAC, at beamline BL15U1 of SSRF ($\lambda = 0.6199$ Å). Daphne 7373 was used as the pressure-transmitting medium. The DIOPTAS program [27] was used for image integrations. The lattice parameters were extracted by using the RIETICA program with Le Bail method [28]. Pressure for all the experiments was calibrated by using the ruby fluorescence method at room temperature [29].

Figure 1 displays the temperature dependence of in-plane resistance (R) for single-crystalline $EuCd_2As_2$ under various pressures up to 49.5 GPa. Starting at 3.4 GPa, the resistance increases monotonically upon cooling from 300 K and shows a peak at $T_N \sim 11$ K, with a change in magnitude of 3–4 orders [Fig. 1(c)]. It drops steeply with further lowering temperature, followed by another slight increase below ~5 K. The whole R-T shape at 3.4 GPa is in line with that of our samples measured at ambient pressure [Fig. 1(b)] and T_N corresponds to an AFM phase transition. The steep resistance drop below T_N is due to reduction of the spin scattering as the AFM state sets in [16,24]. The anomaly below around 5 K is also

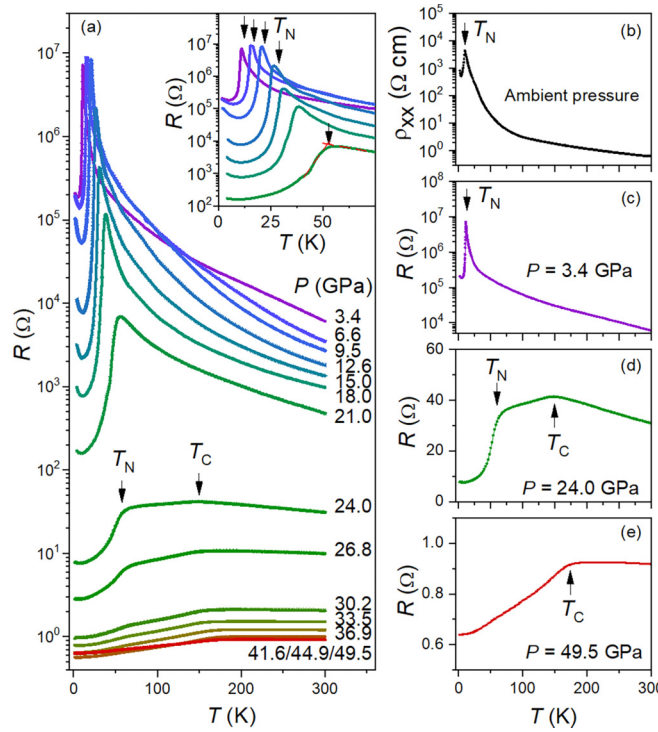

FIG. 1. (a) Temperature dependence of in-plane electric resistance (R) of single-crystal $EuCd_2As_2$ at various pressures up to 49.5 GPa. The sharp peak in resistance as indicated by arrow corresponds to the AFM transition temperature T_N. T_C stands for a magnetic phase transition of FM type as discussed in main text. Inset: Low-temperature R at 3.4–21.0 GPa. (b) Ambient-pressure resistivity (ρ_{XX}) as a function of temperature. (c)–(e) Plots of R-T at 3.4, 24.0, and 49.5 GPa

seen in previous resistivity measurements at ambient pressure [16,25]. This is probably related to redistribution of domain populations as an anomaly in susceptibility is simultaneously observed, which scatters off the charge carriers and enhances the resistance. These results demonstrate a strong coupling between the electrical transport and magnetic properties of $EuCd_2As_2$.

With increasing pressure to 21.0 GPa, T_N shifts to higher temperatures gradually [inset of Fig. 1(a)] and roughly the whole resistance decreases by orders of magnitude. Nevertheless, the shapes of the R-T curves qualitatively resemble each other and keep an insulating conduction behavior with pressure. These observations suggest a stable insulating AFM ground state in the pressure range of 0–21.0 GPa. At 24.0 GPa, a high-temperature kink at $T_C \sim 150$ K in the R-T curve shows up and coexists with the low-temperature AFM-related resistance anomaly at $T_N \sim 55$ K [Fig. 1(d)]. This kink anomaly at T_C can be ascribed to an FM-like transition as discussed below. Upon further compression, the resistance anomaly at T_N gradually fades away and the kink anomaly gets more and more evident with T_C increased slightly. Finally, a dominant FM-like metallic phase is established at 49.5 GPa [Fig. 1(e)], the highest pressure achieved in this experiment.

The temperature dependence of magnetization (M) at pressures to 14.0 GPa is displayed in Fig. 2. At ambient pressure, $EuCd_2As_2$ is an AFM material with $T_N \sim 9.5$ K (inset

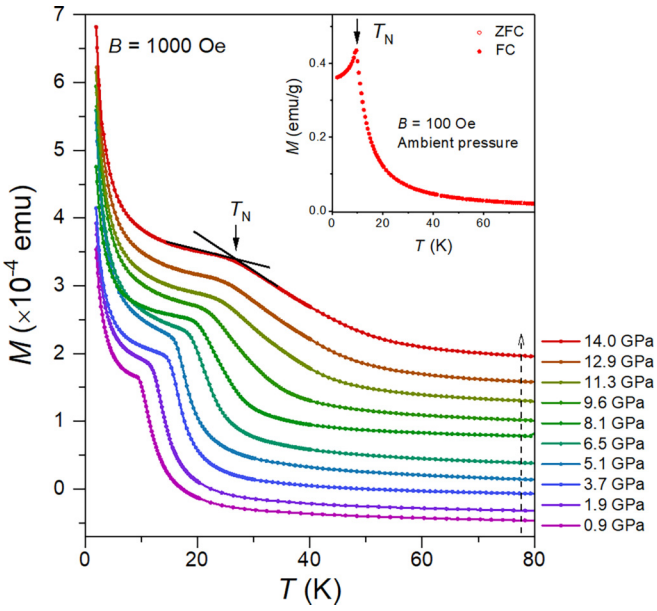

FIG. 2. Magnetization (M) of $EuCd_2As_2$ under high pressure. The AFM transition temperature T_N is determined as the point of intersection of two lines extrapolated from the $M(T)$ curve below and above the temperatures of the broad peak. The applied field is $B = 1000$ Oe. The signals are translated vertically for clarity. Inset shows the M-T curve in a field of $B = 100$ Oe at ambient pressure.

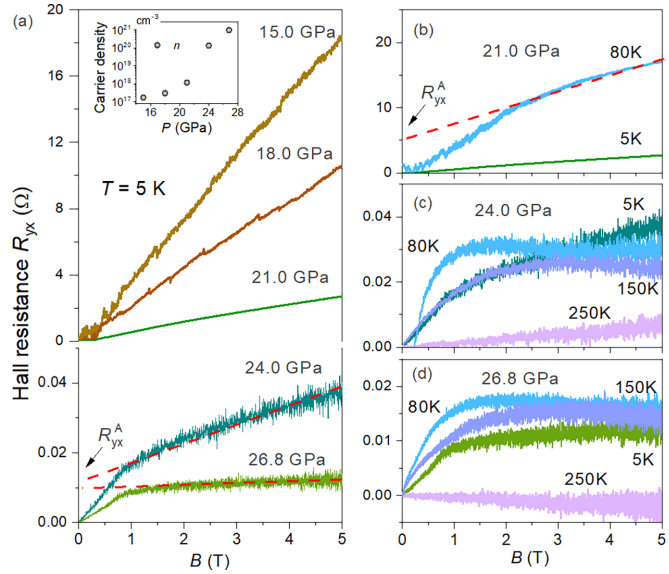

FIG. 3. (a) Hall resistance (R_{yx}) as a function of field (B) at different pressures and a fixed temperature of 5 K. The anomalous Hall resistance (R^A_{yx}) is obtained by linearly extrapolating the high-field part of R_{yx}-B. Inset shows the estimated carrier density n in unit of cm^{-3} versus pressure at 5 K. (b)–(d) R_{yx}-B at different temperatures and pressures. Note that the zero-field R_{yx} at 80 K and 24.0 GPa does not go through the origin due to measurement uncertainty.

of Fig. 2). The measured high-pressure magnetization is a superposition of the weak AFM signal from the tiny mount of samples ($\sim 480 \times 480 \times 80\ \mu m^3$) and the strong paramagnetic background from the BeCu DAC. At 0.9 GPa, a kink anomaly at $T_N \sim 9.6$ K is clearly observed, signifying the AFM phase transition. With increasing pressure, the kink anomaly shifts to higher temperatures monotonically, with the transition broadening slightly due to the pressure gradient across the sample inside the DAC as no pressure medium was used. This indicates pressure-driven enhancement of the antiferromagnetism in the insulating antiferromagnet $EuCd_2As_2$, in agreement with the above transport measurement.

It is instructive to investigate the Hall effect of $EuCd_2As_2$ under pressure. At pressures smaller than 15 GPa, the magnitude of resistance is too large to get a reliable Hall signal. As shown in Fig. 3(a), in the pressure range of 15.0–21.0 GPa we find an ordinary, positive-slope, and roughly linear Hall resistance (R_{yx}) signal in the field range of 0–5 T at 5 K and no evident anomalous Hall effect (AHE), indicating hole-type charge carriers dominating the transport with no polarized FM order even under 5 T. At the same pressure window (18.0–21.0 GPa), the AHE above T_N can be observed, say at 80 K and 21.0 GPa [Fig. 3(b)]. This observation implies the presence of strong FM spin fluctuations or short-range order as seen previously in $EuCd_2As_2$ and its sister compound $EuZn_2As_2$ [13,17,30,31].

With further increasing pressure to 24.0 and 26.8 GPa, clear AHE signals are always observed below $T_C \sim 150$ K [Fig. 3(c)], suggesting the formation of an FM-like state. In addition, a mere ordinary Hall effect (OHE) appears at 250 K since the system enters into a paramagnetic state. The OHE slope at 250 K changes from positive to negative when going from 24.0 to 26.8 GPa, indicating a hole- to electron-type crossover of the dominant carriers [Figs. 3(c) and 3(d)]. This suggests a pressure-induced change of the band structure along with the AFM to FM transition.

At each pressure and 5 K, we fit data of the high-field part from ~1 to 5 T to $\rho_{yx} = R_{yx}t = R_H B$, where t is a fixed sample thickness of 10 μm (before compression) and R_H is a Hall coefficient. By using the Drude relationship for a single-band case with $R_H = -1/ne$, the carrier density n at 5 K can be estimated. As shown in the inset of Fig. 3(a), at 15.0 GPa the carrier density $n \sim 1.7 \times 10^{17}$ cm^{-3} is very low, in line with the insulating nature of $EuCd_2As_2$. Upon further compression, n keeps increasing, consistent with the rapid reduction in magnitude of resistance [Fig. 1(a)].

In order to explore the structural symmetry of $EuCd_2As_2$ under high pressure, we performed synchrotron XRD experiments at room temperature. As shown in Fig. 4(a), the XRD pattern at 0.5 GPa can be well indexed by the ambient-pressure trigonal structure with space group $P\bar{3}m1$ (No. 164). Further compression shifts all peaks to higher angles, in accordance with shrinkage of the lattice. Starting at 28.2 GPa, a tiny peak appears at $2\theta \sim 14°$ (marked by arrow), indicating occurrence of a structural transition. This new structural phase coexists with the pristine one in the pressure range of 28.2–39.9 GPa. As the pressure further goes beyond 39.9 GPa, the XRD patterns are distinctly from those from the low-pressure patterns yet they basically resemble each other, implying completion of the structural transition. The critical pressure of 25.9–28.2 GPa and the observation of a phase coexistence coincide with those observed in the resistance measurement (Fig. 1).

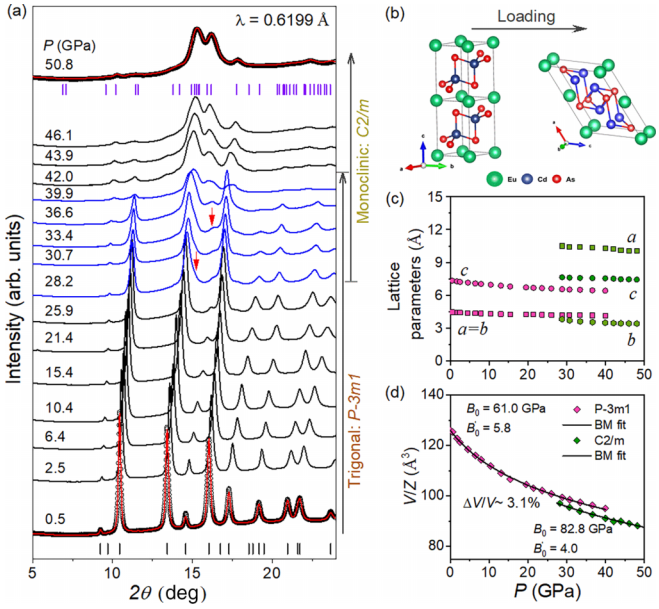

FIG. 4. (a) XRD patterns at selected pressures. The synchrotron radiation x-ray wavelength is $\lambda = 0.6199$ Å. Peaks marked with arrow are from high-pressure phase of $EuCd_2As_2$. (b) Low- and high-pressure lattice structures of $EuCd_2As_2$. (c) Lattice parameters as a function of pressure. The lattice parameters were extracted by using the RIETICA program [28] with Le Bail method. (d) Volume per unit cell V/Z as a function of pressure, i.e., equation of state (EOS). The EOS data were fitted by using the third-order Birch-Murnaghan (BM) model (solid lines). Across the structural transition, the change in volume is about 3.1%, indicating a first-order structural transition.

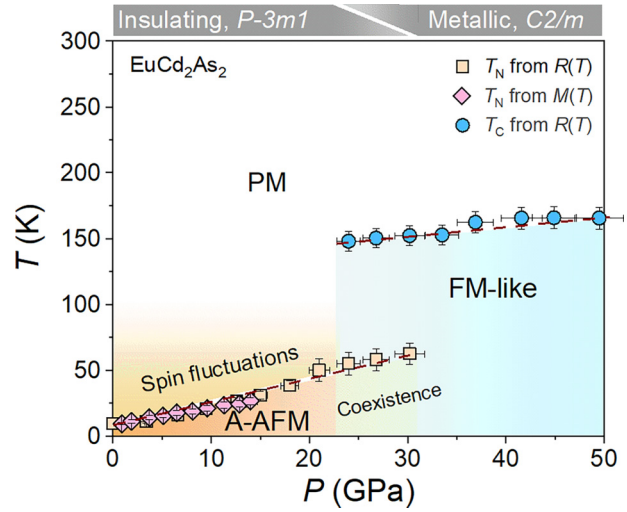

FIG. 5. Temperature-pressure phase diagram for intrinsically insulating antiferromagnet $EuCd_2As_2$. PM, A-AFM, and FM-like are short for the paramagnetic, A-type antiferromagnetic, and ferromagnetic-like states, respectively.

By referencing previous literature [32–35], we found that only the $C2/m$ structure can fit our high-pressure data well [see the upper of Fig. 4(a)]. The lattice structures for these two phases and the extracted lattice parameters are displayed in Figs. 4(b) and 4(c), respectively. The equation of state is fitted by the third-order Birch-Murnaghan equation [36], which gives the bulk modulus $B_0 = 61.0$ GPa and its first-order derivative $B_0' = 5.8$ for the low-pressure $P\bar{3}m1$ phase, and $B_0 = 82.8$ GPa and $B_0' = 4.0$ for the high-pressure $C2/m$ phase [Fig. 4(d)].

We outline the above results into a phase diagram for intrinsically insulating antiferromagnet $EuCd_2As_2$. As shown in Fig. 5, both T_N and T_C increase linearly with pressure at a rate of ~1.90 K/GPa and ~0.69 K/GPa, respectively. The lattice of $EuCd_2As_2$ with a $P\bar{3}m1$ structure is made up of Cd_2As_2 bilayers separated by the triangular Eu layers [Fig. 4(b)]. $EuCd_2As_2$ has an A-type AFM order; i.e., the local $Eu-4f$ moments align ferromagnetically in plane but antiferromagnetically out of plane (along the c axis). While the c axis is compressed easier than the a axis [Fig. 4(c)], the increment of T_N may be dominantly contributed by strengthening of the in-plane FM exchange since the ratio between the nearest-neighbor in-plane FM and out-of-plane AFM exchanges is of order three in magnitude [13]. This is similar to the case observed previously in pressurized $EuIn_2As_2$ [37] and $EuSn_2As_2$ [38].

For metallic $EuCd_2As_2$ samples used in previous literature, pressure-induced A-type AFM to in-plane FM at ~2 GPa and further to possible out-of-plane FM states at ~19–23 GPa was proposed [20–22]. It thus is surprising that for an insulating $EuCd_2As_2$ sample used here, its AFM state is stable against pressure up to 21.0 GPa. This can be indicated by the following arguments: (i) the preservation of the R-T shape with a sharp peak feature and the M-T shape, which means the scatter mechanism keeping unchanged, at least to 14.0 GPa; (ii) the well-matched T_N from different techniques (Fig. 5); (iii) the absence of AHE at 5 K even under 5 T in the pressure range of 15.0–21.0 GPa. Such a sample-dependent evolution of the AFM ground state in $EuCd_2As_2$ may imply that there exist some other mechanisms in affecting its AFM state that have not yet been unveiled.

As discussed above, in the pressure range of 18–21.0 GPa the AHE can be observed above T_N, indicating occurrence of quasi-long-range FM fluctuations [13,31]. Moreover, the anomalous Hall resistivity ($\rho_{yx}^A = R_{yx}^A t$) at 80 K (above T_N) and 21.0 GPa is estimated to ~5 mΩ cm [Fig. 3(b)], which is comparable to those observed in $EuCd_2As_2$ [39] and $Co_3Sn_2S_2$ [40] where the AHE is dictated by the Berry curvature due to nontrivial band topology. This may indicate persistence of nontrivial topological states of $EuCd_2As_2$ up to 21.0 GPa.

When the pressure is increased to 24.0 GPa and above, in addition to the R-T anomaly at $T_N \sim 50$ K relating to the AFM transition, a R-T anomaly at $T_C \sim 150$ K is observed (Fig. 1). Concurrently, the AHE is observed below T_C (including below T_N). Generally, an AHE is typically related to either FM correlations or purely a Berry curvature and spin-orbit coupling in nonmagnetic materials such as in $ZrTe_5$ [41]. For nonmagnetic system, however, the AHE appears below some certain temperature where a magnetic transition is unexpected as there is no magnetic ion and no R-T anomaly is observed. Here, we observed AHE only when $EuCd_2As_2$ is cooled below T_C, indicating a strong correlation between them. The anomaly at T_C cannot be related to a pressure-induced change of Eu^{2+} valence state [21]. These suggest a magnetic origin of the R-T anomaly at T_C, most likely due to a FM-like transition.

In addition, the anomalous Hall resistivity ρ_{yx}^{A} decreases significantly. For example, it decreases from ∼5 mΩ cm at 80 K and 21.0 GPa to ∼0.03 mΩ cm at 80 K and 24.0 GPa. This suggests an abrupt change in band structure of $EuCd_2As_2$ across the magnetic transition. Interestingly, ρ_{yx}^{A} changes nonmonotonically with temperature; meanwhile, the OHE also exhibits a nonmonotonic evolution behavior with temperature and even displays a sign change [Figs. 3(c) and 3(d)]. Origins for these observations are unclear at present. Obviously, further investigations especially from theoretical calculations will be helpful in clarifying these issues.

In summary, we have studied the pressure effect on transport, magnetic, and structural properties of intrinsically insulating antiferromagnet $EuCd_2As_2$. Our data show that the AFM insulating ground state is stable with pressure up to 21.0–24.0 GPa before a FM-like metallic state shows up, owing to a $P\bar{3}m1 \rightarrow C2/m$ structural transition. A temperature-pressure phase diagram for this intrinsic sample is constructed. Our results indicate that the insulating antiferromagnet $EuCd_2As_2$ has nontrivial band topology even above T_N, which may stimulate further research interests on its nature and interplay to transports and magnetism.

The authors are grateful for the financial support from the National Key Research and Development Program of China (Grants No. 2022YFA1602603 and No. 2018YFA0305704), the National Natural Science Foundation of China (Grants No. 12174395, No. U19A2093, No. 12204004, and No. 12004004), and the Users with Excellence Program of Hefei Center CAS (Grant No. 2021HSC-UE008). X.L.C. acknowledges the support from the Open Project of Key Laboratory of Structure and Functional Regulation of Hybrid Materials (Anhui University), Ministry of Education. Y.H.Z. was supported by the Youth Innovation Promotion Association CAS (Grant No. 2020443).

[1] C.-Z. Chang, C.-X. Liu, and A. H. MacDonald, Colloquium: Quantum anomalous Hall effect, Rev. Mod. Phys. **95**, 011002 (2023).

[2] J. H. Li, Y. Li, S. Q. Du, Z. Wang, B.-L. Gu, S.-C. Zhang, K. He, W. H. Duan, and Y. Xu, Intrinsic magnetic topological insulators in van der Waals layered $MnBi_2Te_4$-family materials, Sci. Adv. **5**, eaaw5685 (2019).

[3] C. Liu, Y. Wang, H. Li, Y. Wu, Y. Li, J. Li, K. He, Y. Xu, J. Zhang, and Y. Wang, Robust axion insulator and Chern insulator phases in a two-dimensional antiferromagnetic topological insulator, Nat. Mater. **19**, 522 (2020).

[4] Y. Xu, Z. Song, Z. Wang, H. Weng, and X. Dai, Higher-Order Topology of the Axion Insulator $EuIn_2As_2$, Phys. Rev. Lett. **122**, 256402 (2019).

[5] E. Liu *et al.*, Giant anomalous Hall effect in a ferromagnetic kagome-lattice semimetal, Nat. Phys. **14**, 1125 (2018).

[6] Q. Wang *et al.*, Large intrinsic anomalous Hall effect in half-metallic ferromagnet $Co_3Sn_2S_2$ with magnetic Weyl fermions, Nat. Commun. **9**, 3681 (2018).

[7] L. Šmejkal, Y. Mokrousov, B. H. Yan, and A. H. MacDonald, Topological antiferromagnetic spintronics, Nat. Phys. **14**, 242 (2018).

[8] Y. Tokura, K. Yasuda, and A. Tsukazaki, Magnetic topological insulators, Nat. Rev. Phys. **1**, 126 (2019).

[9] Y. Xu, L. Das, J. Z. Ma, C. J. Yi, S. M. Nie, Y. G. Shi, A. Tiwari, S. S. Tsirkin, T. Neupert, M. Medarde, M. Shi, J. Chang, and T. Shang, Unconventional Transverse Transport above and below the Magnetic Transition Temperature in Weyl Semimetal $EuCd_2As_2$, Phys. Rev. Lett. **126**, 076602 (2021).

[10] J. Krishna, T. Nautiyal, and T. Maitra, First-principles study of electronic structure, transport, and optical properties of $EuCd_2As_2$, Phys. Rev. B **98**, 125110 (2018).

[11] L.-L. Wang, N. H. Jo, B. Kuthanazhi, Y. Wu, R. J. McQueeney, A. Kaminski, and P. C. Canfield, Single pair of Weyl fermions in the half-metallic semimetal $EuCd_2As_2$, Phys. Rev. B **99**, 245147 (2019).

[12] J.-R. Soh, F. de Juan, M. G. Vergniory, N. B. M. Schröter, M. C. Rahn, D. Y. Yan, J. Jiang, M. Bristow, P. Reiss, J. N. Blandy, Y. F. Guo, Y. G. Shi, T. K. Kim, A. McCollam, S. H. Simon, Y. Chen, A. I. Coldea, and A. T. Boothroyd, Ideal Weyl semimetal induced by magnetic exchange, Phys. Rev. B **100**, 201102(R) (2019).

[13] J.-Z. Ma, S. M. Nie, C. J. Yi, J. Jandke, T. Shang, M. Y. Yao, M. Naamneh, L. Q. Yan, Y. Sun, A. Chikina, V. N. Strocov, M. Medarde, M. Song, Y.-M. Xiong, G. Xu, W. Wulfhekel, J. Mesot, M. Reticcioli, C. Franchini, C. Mudry, M. Müller, Y. G. Shi, T. Qian, H. Ding, M. Shi, Spin fluctuation induced Weyl semimetal state in the paramagnetic phase of $EuCd_2As_2$, Sci. Adv. **5**, eaaw4718 (2019).

[14] J. Ma, H. Wang, S. Nie, C. Yi, Y. Xu, H. Li, J. Jandke, W. Wulfhekel, Y. Huang, D. West, P. Richard, A. Chikina, V. N. Strocov, J. Mesot, H. Weng, S. Zhang, Y. Shi, T. Qian, M. Shi, and H. Ding, Emergence of nontrivial low-energy Dirac fermions in antiferromagnetic $EuCd_2As_2$, Adv. Mater. **32**, 1907565 (2020).

[15] K. M. Taddei, L. Lin, L. D. Sanjeewa, Y. Li, J. Xing, C. dela Cruz, D. Phelan, A. S. Sefat, and D. S. Parker, Single pair of Weyl nodes in the spin-canted structure of $EuCd_2As_2$, Phys. Rev. B **105**, L140401 (2022).

[16] M. C. Rahn, J.-R. Soh, S. Francoual, L. S. I. Veiga, J. Strempfer, J. Mardegan, D. Y. Yan, Y. F. Guo, Y. G. Shi, and A. T. Boothroyd, Coupling of magnetic order and charge transport in the candidate Dirac semimetal $EuCd_2As_2$, Phys. Rev. B **97**, 214422 (2018).

[17] J.-R. Soh, E. Schierle, D. Y. Yan, H. Su, D. Prabhakaran, E. Weschke, Y. F. Guo, Y. G. Shi, and A. T. Boothroyd, Resonant x-ray scattering study of diffuse magnetic scattering from the topological semimetals $EuCd_2As_2$ and $EuCd_2Sb_2$, Phys. Rev. B **102**, 014408 (2020).

[18] N. H. Jo, B. Kuthanazhi, Y. Wu, E. Timmons, T.-H. Kim, L. Zhou, L.-L. Wang, B. G. Ueland, A. Palasyuk, D. H. Ryan, R. J. McQueeney, K. Lee, B. Schrunk, A. A. Burkov, R. Prozorov, S. L. Bud'ko, A. Kaminski, and P. C. Canfield, Manipulating magnetism in the topological semimetal $EuCd_2As_2$, Phys. Rev. B **101**, 140402(R) (2020).

[19] L. D. Sanjeewa, J. Xing, K. M. Taddei, D. Parker, R. Custelcean, C. dela Cruz, and A. S. Sefat, Evidence of Ba-substitution induced spin-canting in the magnetic Weyl semimetal $EuCd_2As_2$, Phys. Rev. B **102**, 104404 (2020).

[20] F. Du, L. Yang, Z. Nie, N. Wu, Y. Li, S. Luo, Y. Chen, D. Su, M. Smidman, Y. Shi, C. Cao, F. Steglich, Y. Song, and H. Yuan, Consecutive topological phase transitions and colossal magnetoresistance in a magnetic topological semimetal, npj Quantum Mater. **7**, 65 (2022).

[21] Z. Yu, X. Chen, W. Xia, N. Wang, X. Lv, X. Liu, H. Su, Z. Li, D. Wu, W. Wu, Z. Liu, J. Zhao, M. Li, S. Li, X. Li, Z. Dong, C. Zhou, L. Zhang, X. Wang, N. Yu, *et al.*, Pressure-induced ideal Weyl semimetal state in the layered antiferromagnet $EuCd_2As_2$, arXiv:2202.06016.

[22] E. Gati, S. L. Bud'ko, L.-L. Wang, A. Valadkhani, R. Gupta, B. Kuthanazhi, L. Xiang, J. M. Wilde, A. Sapkota, Z. Guguchia, R. Khasanov, R. Valentí, and P. C. Canfield, Pressure-induced ferromagnetism in the topological semimetal $EuCd_2As_2$, Phys. Rev. B **104**, 155124 (2021).

[23] S. K. Kushwaha, I. Pletikosic, T. Liang, A. Gyenis, S. H. Lapidus, Y. Tian, H. Zhao, K. S. Burch, J. J. Lin, W. D. Wang, H. W. Ji, A. V. Fedorov, Ali Yazdani, N. P. Ong, T. Valla, and R. J. Cava, Sn-doped $Bi_{1.1}Sb_{0.9}Te_2S$ bulk crystal topological insulator with excellent properties, Nat. Commun. **7**, 11456 (2016).

[24] H. P. Wang, D. S. Wu, Y. G. Shi, and N. L. Wang, Anisotropic transport and optical spectroscopy study on antiferromagnetic triangular lattice $EuCd_2As_2$: An interplay between magnetism and charge transport properties, Phys. Rev. B **94**, 045112 (2016).

[25] D. Santos-Cottin, I. Mohelsky, J. Wyzula, F. Le Mardele, I. Kapon, S. Nasrallah, N. Barisic, I. Zivkovic, J. R. Soh, F. Guo, M. Puppin, J. H. Dil, B. Gudac, Z. Rukelj, M. Novak, A. B. Kuzmenko, C. C. Homes, Tomasz Dietl, M. Orlita, and Ana Akrap, $EuCd_2As_2$: A magnetic semiconductor, arXiv:2301.08014.

[26] X. L. Chen, D. X. Shao, C. C. Gu, Y. H. Zhou, C. An, Y. Zhou, X. D. Zhu, T. Chen, M. L. Tian, J. Sun, and Z. R. Yang, Pressure-induced multiband superconductivity in pyrite $PtBi_2$ with perfect electron-hole compensation, Phys. Rev. Mater. **2**, 054203 (2018).

[27] C. Prescher and V. B. Prakapenka, DIOPTAS: A program for reduction of two-dimensional x-ray diffraction data and data exploration, High Pressure Res. **35**, 223 (2015).

[28] B. A. Hunter, RIETICA-A Visual Rietveld Program, International Union of Crystallography Commission on Powder Diffraction, Newsletter No. 20 (Summer 1998), http://www.rietica.org.

[29] H. K. Mao, J. Xu, and P. M. Bell, Calibration of the ruby pressure gauge to 800 kbar under quasi-hydrostatic conditions, J. Geophys. Res. **91**, 4673 (1986).

[30] J. Blawat, M. Marshall, J. Singleton, E. Feng, H. Cao, W. Xie, and R. Jin, Unusual electrical and magnetic properties in layered $EuZn_2As_2$, Adv. Quantum Technol. **5**, 2200012 (2022).

[31] E. Yi, D. F. Zheng, F. Pan, H. Zhang, B. Wang, B. Chen, D. Wu, H. Liang, Z. X. Mei, H. Wu, S. A. Yang, P. Cheng, M. Wang, and B. Shen, Topological Hall effect driven by short-range magnetic order in $EuZn_2As_2$, Phys. Rev. B **107**, 035142 (2023).

[32] S. Strikos, B. Joseph, F. G. Alabarse, G. Valadares, D. G. Costa, R. B. Capaz, and M. ElMassalami, Pressure dependence of room-temperature structural properties of $CaAl_2Si_2$, J. Phys.: Condens. Matter **32**, 365403 (2020).

[33] J. F. Rauscher, C. L. Condron, T. Beault, S. M. Kauzlarich, N. Jensen, P. Klavins, S. MaQuilon, Z. Fisk, and M. M. Olmstead, Flux growth and structure of two compounds with the $EuIn_2P_2$ structure type, AIn_2P_2 (A = Ca and Sr), and a new structure type, $BaIn_2P_2$, Acta Crystallogr., Sect. C: Cryst. Struct. Commun. **65**, i69 (2009).

[34] X. Gui, G. J. Finkelstein, K. Y. Chen, T. Yong, P. Dera, J. G. Cheng, and W. W. Xie, Pressure-induced large volume collapse, plane-to-chain, insulator to metal transition in $CaMn_2Bi_2$, Inorg. Chem. **58**, 8933 (2019).

[35] L. Zhao, C. J. Yi, C.-T. Wang, Z. H. Chi, Y. Y. Yin, X. L. Ma, J. H. Dai, P. T. Yang, B. B. Yue, J. G. Cheng, F. Hong, J.-T. Wang, Y. H. Han, Y. G. Shi, and X. H. Yu, Monoclinic $EuSn_2As_2$: A Novel High-Pressure Network Structure, Phys. Rev. Lett. **126**, 155701 (2021).

[36] F. Birch, Finite elastic strain of cubic crystals, Phys. Rev. **71**, 809 (1947).

[37] F. H. Yu, H. M. Mu, W. Z. Zhuo, Z. Y. Wang, Z. F. Wang, J. J. Ying, and X. H. Cheng, Elevating the magnetic exchange coupling in the compressed antiferromagnetic axion insulator candidate $EuIn_2As_2$, Phys. Rev. B **102**, 180404(R) (2020).

[38] H. L. Sun, C. Q. Chen, Y. S. Hou, Y. Gong, M. W. Huo, L. S. Li, J. Yu, W. P. Cai, N. T. Liu, R. Q. Wu, D.-X. Yao, and M. Wang, Various magnetism of the compressed antiferromagnetic topological insulator $EuSn_2As_2$, Sci. China: Phys., Mech. Astron. **64**, 118211 (2021).

[39] M. Ohno, S. Minami, Y. Nakazawa, S. Sato, M. Kriener, R. Arita, M. Kawasaki, and M. Uchida, Maximizing intrinsic anomalous Hall effect by controlling the Fermi level in simple Weyl semimetal films, Phys. Rev. B **105**, L201101 (2022).

[40] X. Chen, M. Wang, C. Gu, S. Wang, Y. Zhou, C. An, Y. Zhou, B. Zhang, C. Chen, Y. Yuan, M. Qi, L. Zhang, H. Zhou, J. Zhou, Y. Yao, and Z. Yang, Pressure-tunable large anomalous Hall effect of the ferromagnetic kagome-lattice Weyl semimetal $Co_3Sn_2S_2$, Phys. Rev. B **100**, 165145 (2019).

[41] T. Liang, J. Lin, Q. Gibson, S. Kushwaha, M. Liu, W. Wang, H. Xiong, J. A. Sobota, M. Hashimoto, P. S. Kirchmann, Z.-X. Shen, R. J. Cava, and N. P. Ong, Anomalous Hall effect in $ZrTe_5$, Nat. Phys. **14**, 451 (2018).